X-ray structure of a native calicivirus: Structural insights into antigenic diversity and host specificity

Rong Chen*†, John D. Neill‡, Mary K. Estes§, and B. V. Venkataram Prasad*§¶

*Verna and Marrs McLean Department of Biochemistry and Molecular Biology and §Department of Molecular Virology and Microbiology, Baylor College of Medicine, Houston, TX 77030; and ‡National Animal Disease Center, Agriculture Research Service, U.S. Department of Agriculture, Ames, IA 50010

Edited by Bernard Roizman, University of Chicago, Chicago, IL, and approved April 14, 2006 (received for review January 17, 2006)

Caliciviruses, grouped into four genera, are important human and veterinary pathogens with a potential for zoonosis. In these viruses, capsid-related functions such as assembly, antigenicity, and receptor interactions are predominantly encoded in a single protein that forms an icosahedral capsid. Understanding of the immunologic functions and pathogenesis of human caliciviruses in the *Norovirus* and *Sapovirus* genera is hampered by the lack of a cell culture system or animal models. Much of our understanding of these viruses, including the structure, has depended on recombinant capsids. Here we report the atomic structure of a native calicivirus from the *Vesivirus* genus that exhibits a broad host range possibly including humans and map immunological function onto a calicivirus structure. The vesivirus structure, despite a similar architectural design as seen in the recombinant norovirus capsid, exhibits novel features and indicates how the unique modular organization of the capsid protein with interdomain flexibility, similar to an antibody structure with a hinge and an elbow, integrates capsid-related functions and facilitates strain diversity in caliciviruses. The internally located N-terminal arm participates in a novel network of interactions through domain swapping to assist the assembly of the shell domain into an icosahedral scaffold, from which the protruding domain emanates. Neutralization epitopes localize to three hypervariable loops in the distal portion of the protruding domain surrounding a region that exhibits host-specific conservation. These observations suggest a mechanism for antigenic diversity and host specificity in caliciviruses and provide a structural framework for vaccine development.

neutralization epitopes | norovirus | vesivirus

Caliciviridae is a family of positive sense single-stranded RNA viruses comprised of both human and animal pathogens. These viruses are phylogenetically divided into four genera: *Norovirus*, *Sapovirus*, *Lagovirus*, and *Vesivirus* (1). Viruses in the first two genera, *Norovirus* and *Sapovirus*, are mostly human pathogens and are the major causative agents of acute, epidemic, nonbacterial gastroenteritis (2, 3). Recent studies have indicated the inclusion of bovine and porcine viruses in these genera and suggested the potential existence of animal reservoirs and the possibility of interspecies transmission (4–8). Viruses in the other two genera, *Lagovirus* and *Vesivirus*, are animal pathogens of veterinary importance (9). These viruses, particularly vesiviruses, infect a number of animal species and cause host-specific diseases such as gastroenteritis, vesicular lesions, reproductive failure, and hemorrhagic disease. It is suggested that some vesiviruses from oceanic reservoirs have emerged as terrestrial animal pathogens (10). One of the serotypes of San Miguel sea lion virus (SMSV), belonging to the *Vesivirus* genus, has a list of several natural hosts, including five genera of seals, cattle, three genera of whales, donkeys, foxes, and humans (10, 11). A zoonotic potential of SMSV and feline calicivirus (FCV), a member of the *Vesivirus* genus and a major causative agent of upper respiratory and hemorrhagic diseases in cats (12), is suggested by reports of human antibody against these viruses (10, 11, 13). Our aim in this study was to provide a structural characterization of a prototype vesivirus and examine the extent of structural complementarity between animal and human caliciviruses.

Human caliciviruses (*Norovirus* and *Sapovirus*) are refractory to *in vitro* cultivation in cells, and understanding of their immunologic functions and pathogenesis is hampered by a lack of suitable animal models. Much of our understanding of these viruses in terms of their molecular biology, structure, and immunology has been made possible by the use of recombinant virus-like particles (14–16). In contrast, vesiviruses are readily cultivatable *in vitro*, and there is a significant amount of immunological data for some of these pathogens, including the locations of neutralization epitopes (17–21). Mapping of these sites onto the capsid structure would be useful in providing a structural basis of antigenic functions not only in these viruses but possibly in human caliciviruses. However, there is no high-resolution structure of any vesivirus to date. The only x-ray crystallographic structure available of a calicivirus is that of the recombinant capsid of Norwalk virus (rNV), a human pathogen in the *Norovirus* genus (16). Here we report the x-ray structure of SMSV, a prototype member of the *Vesivirus* genus, which exhibits the broadest host range among caliciviruses.

In all caliciviruses, the genomic RNA (≈8 kb) encodes a major capsid protein, VP1 (55–70 kDa); a putative minor structural protein, VP2; and a large polyprotein, which is posttranslationally processed into nonstructural proteins that are essential for virus replication (22–24). The major capsid protein VP1 is responsible for most of the capsid-related functions such as assembly, host interactions, and immunogenicity. The role of VP2, whose presence in the virion has been demonstrated so far only in rabbit hemorrhagic disease virus, Norwalk virus (NV), and FCV, is unclear. A distinguishing feature of the vesivirus genome, in contrast to that in other caliciviruses, is that it encodes a capsid protein precursor (73–78 kDa) that is proteolytically processed by the viral protease to yield a mature capsid protein of ≈60 kDa (25), which is significantly larger in size than the capsid protein (≈55 kDa) of human caliciviruses. Cryo-EM structural studies on various caliciviruses have shown that their capsids exhibit a T=3 icosahedral symmetry consisting of 90 dimers of the major capsid protein (26–28). Despite capsid architecture and domain organization similar to those in the rNV (16), the x-ray crystallographic structure of SMSV shows significant and distinct variations, some of which may be important for host specificity and antigenic diversity.

Conflict of interest statement: No conflicts declared.

This paper was submitted directly (Track II) to the PNAS office.

Abbreviations: SMSV, San Miguel sea lion virus; NTA, N-terminal arm; NV, Norwalk virus; rNV, recombinant capsid of NV; FCV, feline calicivirus; HVR, hypervariable region; S domain, shell domain; P domain, protruding domain; NT, N-terminal; CT, C-terminal.

Data deposition: The atomic coordinates have been deposited in the Protein Data Bank, www.pdb.org (PDB ID code 2GH8).

†Present address: Department of Medicine, Microbiology, and Molecular Genetics, Brigham and Women's Hospital and Harvard Medical School, Boston, MA 02115.

¶To whom correspondence should be addressed. E-mail: vprasad@bcm.tmc.edu.

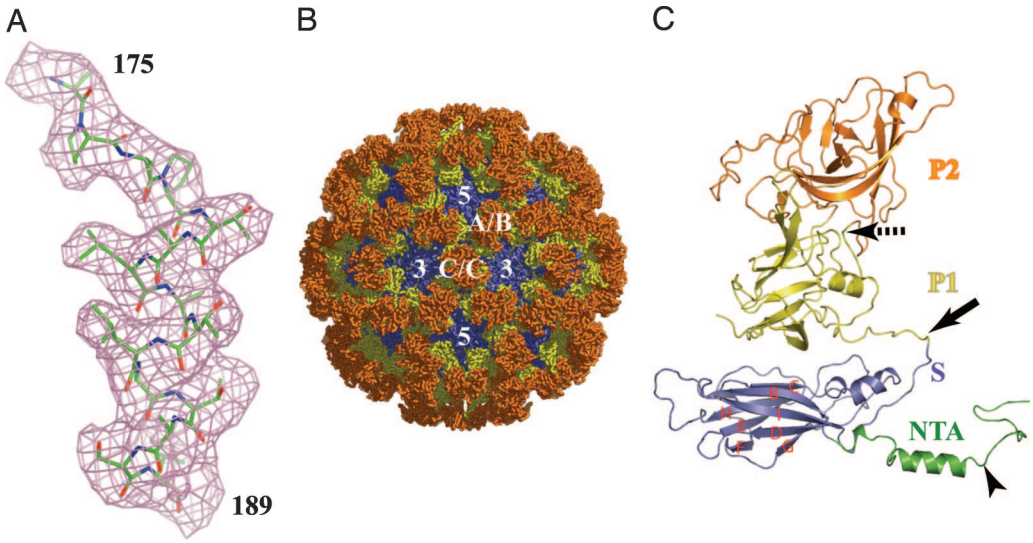

Fig. 1. X-ray structure of SMSV. (*A*) A sample region in the electron density map with modeled amino acid residues 175–189 (APAPTALATLATAST). (*B*) The x-ray structure of SMSV viewed along the icosahedral twofold axis (capsid protein subunits are shown as Cα trace). Locations of a set of A/B and C/C dimers and icosahedral fivefold and threefold axes are denoted. The NTA (internal, not visible in this view), S domain, and P1 and P2 subdomains of the subunits are colored in green, blue, yellow, and orange, respectively. (*C*) A ribbon representation of the B subunit structure. The NTA (residues 163–200, green), S domain (residues 201–361, blue), and P1 (residues 362–413 and 590–703, yellow) and P2 (residues 414–589, orange) subdomains are indicated. BIDG and CHEF β-strands in the S domain are denoted. The arrowhead indicates the location of the Pro-178; solid and dashed arrows indicate the location of the hinge (residues 359–361) between the S and P domains and the location of a strictly conserved Gly-414 at the P1/P2 junction, respectively. The sequence–structure relations for SMSV (along with that in rNV for comparison) are shown in Fig. 5, which is published as supporting information on the PNAS web site.

Results

T=3 Icosahedral Structure of SMSV. The crystal structure of SMSV (serotype 4) was determined to 3.2-Å resolution by molecular replacement techniques by using a 19-Å cryo-EM map of SMSV (28) as an initial phasing model (Fig. 1). As in other T=3 viruses, the icosahedral asymmetrical unit in the SMSV capsid structure (Fig. 1*B*) consists of three quasiequivalent subunits, designated as A, B, and C following the standard nomenclature (29). The A and B subunits form dimers (A/B) across the local twofold axes that surround a large hollow at the fivefold axes of the T=3 icosahedral lattice. At the icosahedral twofold axes, two C subunits interact with each other to form C/C dimers. The A/B and C/C dimers alternate around the hollows at the icosahedral threefold axis. In subunits A, B, and C the electron density is visible for residues 160–703 (following the residue numbering of the precursor capsid protein), 163–703, and 160–703, respectively. The cleavage site in the precursor capsid protein has not been experimentally identified for SMSV. Based on the identified cleavage sites in feline (30) and canine (31) calicivirus capsid protein precursors and sequence alignments, Glu-152–Ser-153 is likely the cleavage site in SMSV. If Ser-153 is the first residue in the capsid protein, then seven, ten, and seven N-terminal residues are disordered in the A, B, and C subunits, respectively, in addition to seven residues at the C terminus in all of the subunits. The RNA genome and the putative minor structural protein (VP2) are not visible in the electron density map. The structure of each subunit (Fig. 1*C*) comprises an N-terminal arm (NTA), a shell domain (S domain), and a protruding domain (P domain), similar to that seen in rNV (16).

Unique NTA Interactions. In many T=3 virus capsids, the NTA is suggested to provide a switch to distinguish bent A/B and flat C/C dimers during T=3 icosahedral assembly (29, 32). The structure of SMSV exhibits a novel and distinct variation from any of these viruses. The NTAs of all of the three subunits in the icosahedral asymmetric unit of SMSV are equally ordered and provide a network of interactions essentially maintaining the T=3 icosahedral symmetry at this level (Fig. 2*A*). The NTAs of A, B, and C subunits traverse beneath the S domains of their opposing dimeric partners forming extensive domain-swapping interactions with the S domains (Fig. 2*B*). The NTAs of the A and C subunits terminate close to the icosahedral threefold axis, whereas the NTA of the B subunit terminates close to the fivefold axis and interacts cyclically with the other (fivefold-related) B subunit NTAs through hydrogen bonding to form a distinct ring-like structure.

Although the structures of the NTA of all of the three subunits are similar from residue 178 to residue 212 with a well defined α-helix, the polypeptide chain from residue 162 to residue 178 in the B subunit deviates significantly compared with that in the A and C subunits. This deviation, brought about by the residue Pro-178 (Fig. 1*C*, arrowhead), which changes conformation from the α-region (psi = −47°) seen in the A and C subunits to the β region (psi = 150°) seen in the B subunit, facilitates the formation of the ring-like structure around the fivefold axes. Another rather unusual interaction is at the local threefold axis, where the α-helices of the NTAs from the neighboring twofold-related asymmetric units interact closely through hydrophobic interactions (Fig. 2*B*).

The S Domain Provides an Icosahedral Scaffold. The S domain, formed by residues 201–361, folds into a canonical eight-stranded β-barrel, a structural feature commonly seen in many other viral capsid proteins (29, 32). These eight strands (denoted as B-I) form two four-stranded antiparallel sheets, BIDG and CHEF, with two α-helices between the strands C and D and strands E and F, respectively (Fig. 1*C*). In each subunit, the G strand of the BIDG sheet interacts with the N-terminal loop of the NTA from the opposing subunit related by the dimeric twofold axis. The icosahedral shell is stabilized exclusively by the intersubunit interactions between the trapezoidal-shaped 180 S domains and their NTAs as described above. Like in other T=3 icosahedral shells, the S domains in the A/B and C/C dimers exhibit bent and flat conformations, respectively. The formation of the closed icosahedral shell forces small changes seen in the

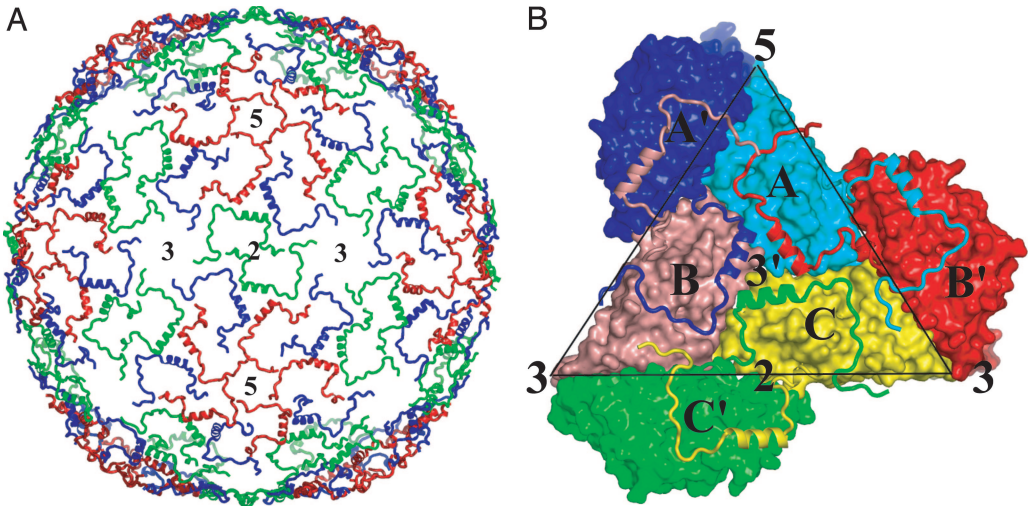

Fig. 2. The NTAs of SMSV form a novel network of interactions. (*A*) The network of interactions among NTAs of subunits A, B, and C (colored in blue, red, and green, respectively) in the SMSV capsid. The icosahedral fivefold, threefold, and twofold axes are denoted. (*B*) A view from inside of the capsid showing domain-swapping interactions between the twofold-related subunits (A′B, CC′, and AB′) and hydrophobic interactions at the local threefold axis between the α-helices from the subunits belonging to neighboring asymmetric units. The icosahedral and the local threefold axis are labeled as 5, 3, 2, and 3′, respectively. The S domains of the A, B, and C subunits (slate, orange, and yellow, respectively) in an icosahedral asymmetric unit and their dimer-related subunits (B′, A′, and C′ in red, blue, and green) are shown as surface representations, whereas their respective NTAs in the same colors are shown as ribbons.

relative orientations of the P domains with respect to the S domains in the A, B, and C subunits. These changes are facilitated by a flexible hinge that joins the S and P domains (Fig. 1*C*, solid arrow). In the B subunit, the P–S orientation brings the C-terminal residues of the P domain closer to the upper portion of the S domain to facilitate interdomain hydrogen bond interactions that may further stabilize the bent conformation of the A/B dimer. In the C/C dimers such P–S interactions are absent.

The P Domain. The P domain, comprising residues 362–703, can be divided into two distinct subdomains, P1 and P2, as in the rNV subunit structure (16). The P domains participate solely in the dimeric interactions across the local (A/B dimer) and strict (C/C dimer) twofold axes. The P1 subdomain, formed by two noncontiguous segments of the polypeptide (residues 362–413 and 590–703), exhibits a fold similar to that seen in rNV. This fold, composed of a twisted β-sheet formed by the four strands in the C-terminal portion of P1 and a lone α-helix, is not seen in other proteins and appears to be a characteristic feature of caliciviruses. However, in SMSV the β-sheet is less twisted and the α-helix is oriented slightly differently when compared with rNV (Fig. 3). In addition, compared with rNV, the orientation of the P1 subdomain with respect to the S domain in SMSV is significantly altered. This change in S–P1 orientation together with a compensatory change in P1–P2 orientation causes only the distal P2 subdomain to participate in the dimeric interactions in contrast to that seen in rNV, where both P1 and P2 subdomains are involved in dimeric interactions (Fig. 3 *A* and *B*). A conserved glycine located at the junction of P1 and P2 appears to be involved in facilitating this compensatory change in the P1–P2 orientation (Fig. 1*C*, dashed arrow). Thus, in addition to the flexibility between the S and P1 domains, the structure of SMSV indicates an additional point of flexibility between the P1 and P2 subdomains.

The P2 Subdomain Is a Large Insertion in the P1. The P2 subdomain is formed by residues 414–589, which are between the two

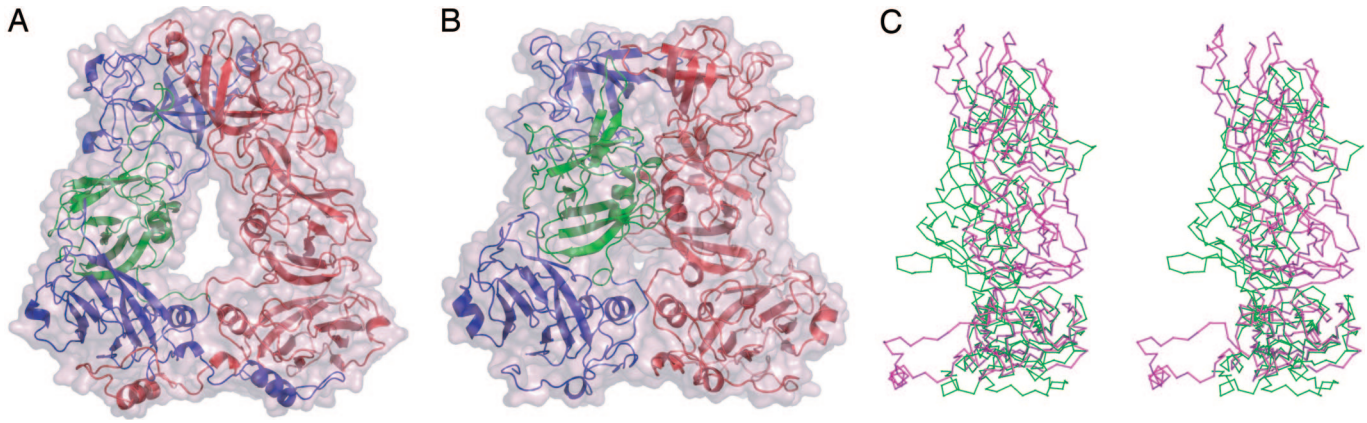

Fig. 3. Dimer interactions and interdomain orientations. The dimeric interactions in the A/B dimers of SMSV (*A*) and rNV (*B*) structures (Protein Data Bank ID code 1IHM). Ribbon representations of the AB subunits involved in the dimeric interactions are shown within a semitransparent surface of the dimer; in each case the P1 subdomain in the A subunit is highlighted in green, whereas the rest of the structure is shown in blue, and the B subunit in each case is shown in red. (*C*) Stereo view of the superposition of the SMSV (magenta) and rNV (green) subunit structures, indicating significant changes in the interdomain orientations between the two structures.

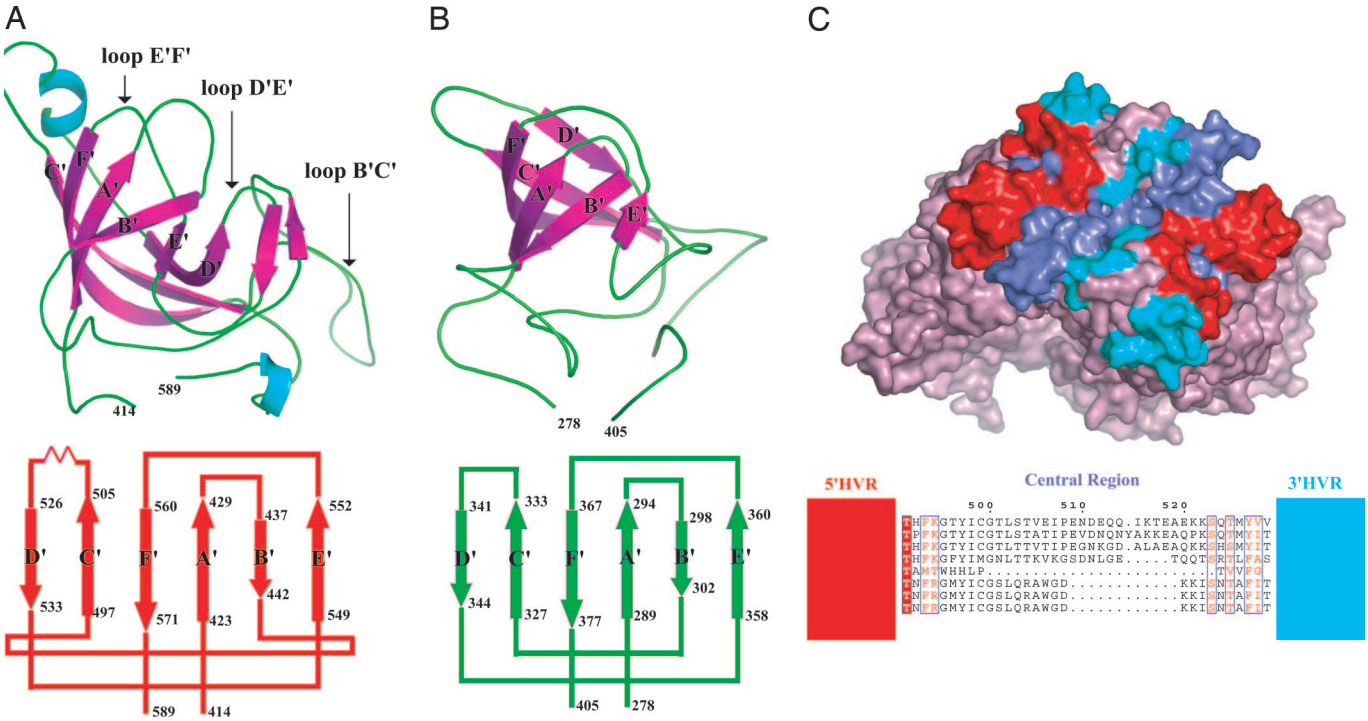

Fig. 4. Structure of the P2 subdomain and mapping of the FCV neutralizations sites. Ribbon representations (*Upper*) of the P2 subdomains in SMSV (*A*) and rNV (*B*) along with their respective topology diagrams (*Lower*). The β-strands are labeled from A′ to F′ in each case. The loops containing the FCV neutralization epitopes are indicated for SMSV. (*C Upper*) Surface representation of the A/B dimer as viewed from outside the capsid (approximately along the dimeric twofold axis) showing the N-terminal (NT) HVR, central conserved region, and C-terminal (CT) HVR in red, blue, and cyan, respectively. (*C Lower*) Sequence comparison of the representative sequences from SMSV (top four sequences corresponding to SMSV4, SMSV5, primate, and SMSV1), canine calicivirus, and FCV (bottom three sequences corresponding to FCV6, FCV4, and FCV9) in the conserved region flanked by the NT and CT HVRs showing host-dependent conservation (see also Fig. 6).

polypeptide segments that form the P1 subdomain (Fig. 4). Thus, the P2 subdomain can be considered as a large insertion in the P1 subdomain. The P2 subdomain contains a compact barrel of six β-strands connected by loops of various lengths. Despite a low sequence similarity, strikingly, these six strands, labeled A′–F′, are spatially arranged in a similar manner as in the rNV capsid protein (Fig. 4 *A* and *B*). However, the P2 subdomain of SMSV contains ≈50 more residues than that in rNV. The "inserted" residues are mainly distributed in the loops connecting these β-strands. The loop linking strands B′ and C′ alone contains ≈30 more residues than its counterpart region in rNV. The loop connecting the strands C′ and D′ in SMSV also has a significant insertion of ≈10 residues. The conservation of the polypeptide fold in the P2 subdomain across two genera despite weak sequence homology strongly suggests that this fold is conserved in all caliciviruses.

Neutralization Antigenic Sites Maps to P2 Subdomain. Several studies have indicated that the hypervariable P2 subdomain plays an important role in antigenicity and receptor interactions in both human and animal caliciviruses (17–21, 33–35). Antigenic properties and mechanism of pathogenesis in human caliciviruses are difficult to characterize because of the lack of a cultivation system. In contrast, for some vesiviruses, such as FCV and canine calicivirus, neutralization-resistant mutants are isolated and characterized (18, 36). Sequence comparison and secondary structure predictions for the capsid proteins of these two viruses indicate that they most likely exhibit structures similar to SMSV, and this structure could provide a structural framework for understanding the antigenicity in these viruses. Several studies using recombinant peptides and domain swaps have shown that the neutralization epitopes in FCV reside in a hypervariable region (HVR) of the sequence encompassing residues 408–529 (FCV numbering according to F9) (17, 19, 21) (see Fig. 6, which is published as supporting information on the PNAS web site). This region maps exclusively to the P2 subdomain in the SMSV structure. Subsequent studies mapped these sites to two smaller regions of hypervariability, NT HVR (426–460) and CT HVR (489–523), and a relatively conserved region between residues 460 and 489. The NT HVR epitope, which is the major immunogenic domain containing at least two linear B cell epitopes (20), maps to a highly exposed long loop connecting B′ and C′ strands (Fig. 4*A*). This loop is noticeably shorter in the rNV structure. The CT HVR maps to two other loops between D′ and E′ and between E′ and F′ (Fig. 4*A*), consistent with the observation that epitopes in this region are conformational. Both of these regions are exposed and easily accessible from the outside (Fig. 4*C Upper*). Thus, the loops of the conserved β-barrel fold in the P2 subdomain represent the immunodominant regions in caliciviruses and facilitate antigenic diversity.

The conserved region flanked by the NT and CT HVRs maps to the dimeric interface and thus may be essential for maintaining the structural integrity in this region (Fig. 4*C Upper*). One of the linear B cell epitopes in FCV maps to this region (20). One FCV monoclonal antibody (1D7), which neutralizes all FCV strains tested, is suggested to bind to this region (21). The sequence conservation seen in this region is not across all caliciviruses but is host-dependent. That is, this region is highly conserved within FCV and SMSV strains, respectively, but not between them. This region is also relatively well conserved within noroviruses. Sequence alignment of FCV, canine calicivirus, and SMSV indicate that FCV and canine calicivirus have a deletion that corresponds to a surface loop in this region (Fig. 4*C Lower*). In noroviruses, the residues that are suggested to be involved in the binding of carbohydrates, putative norovirus receptors, using evolutionary trace analysis and mutational

BIOCHEMISTRY

studies localize in this region (33–35). A distinct possibility is that this region, which shows species-dependent conservation, may be involved in host-specific receptor interactions.

Discussion

In caliciviruses, the capsid-related functions such as assembly, antigenicity, and host specificity are predominantly encoded in one single gene product. The present structure of SMSV, in the *Vesivirus* genus, and that of rNV (16), in the *Norovirus* genus, demonstrate how these functions are integrated into one capsid protein through a unique modular domain organization. Based on these representative x-ray structures from two calicivirus genera, cryo-EM structures of various caliciviruses (26–28), and sequence comparisons (although it is very likely that all caliciviruses exhibit similar T=3 capsid architecture and subunit domain organization), significant variations within the subunit should be expected as demonstrated by the SMSV structure.

One variation seen in the SMSV structure, which is distinct not only from the NV capsid but also from other T=3 (or P=3) capsids, is in the intersubunit interactions involving the NTAs. In these capsids, the NTA is implicated in providing a switch to facilitate bent and flat conformations of the subunit dimers during T=3 capsid assembly (32), which is likely the case in SMSV also. In contrast to what is observed in the case of SMSV in which the NTAs of A, B, and C are equally ordered, in many of the structurally characterized T=3 capsids, such as sobomaviruses (37), tombus viruses (38, 39), nodaviruses (40), and NV (16), at the level of the NTA, the T=3 icosahedral symmetry is reduced to T=1 with only one of the three NTAs being ordered. In plant tombus and sobamoviruses, the NTA of the C subunit is ordered, whereas the equivalent regions in the A and B subunits are disordered, providing a switch to allow bent and flat conformations of the A/B and C/C dimers, respectively (37–39). In rNV, the ordered NTA of the B subunit, which interacts with the base of the S domain of the neighboring C subunit, is suggested to provide such a switch (16). In nodaviruses, an ordered arm of the C subunit and a piece of genomic RNA are implicated in keeping the flat conformation of the C/C dimers (40). In the case of SMSV, instead of such an order-to-disorder transition, a distinct conformational change involving a Pro residue in the B subunit leading to a formation of a ring-like structure around the fivefold axis appears to provide a switch. Whether these unique NTA interactions in SMSV are influenced by the genome or the proteolytic processing of the capsid protein remains a question.

In addition to its role in providing a switch during assembly, the elaborate network of NTA interactions suggests an extensive role in directing the assembly pathway. The assembly pathway, likely initiated from a dimer, stabilized by the intradimeric domain-swapping interactions involving NTAs and other interactions involving S and P2 domains, proceeds through the formation of trimers of dimers, stabilized by the interactions between the NTA α-helices at the local threefold axes. These trimers of dimers are then brought together into an icosahedral structure through the formation of the ring-like structure at the icosahedral fivefold axes involving the NTAs of the B subunits. In this process, the change in the conformation of the B subunit NTA resulting in the ring-like structure may function like a switch to induce/stabilize the bent conformation in the A/B dimer necessary for forming the appropriate curvature.

Although the polypeptide fold of the S domain in SMSV and the icosahedral shell formed by the close association of S domains is very similar to other T=3 (P=3) icosahedral capsids, the fold of the P domain is quite unique and thus far seen only in the NV structure. In plant tombus viruses (16, 38, 39), which also have well defined P domains, their structures are quite different from that seen in SMSV or NV. The main difference between the P domains of NV and SMSV, both having two subdomains, P1 and P2, is in the relative orientation of the P domain with respect to the S domain. The flexible hinge between the S and P domain in SMSV, at the interface of S and P1, is similar to that observed in the plant tombus virus (38, 39) and the rNV capsid structure (16). This hinge, which facilitates the interactions between the P1 subdomain and the upper portion of the S domain, may be important for "holding" the A/B and C/C dimers in appropriate conformations, because this interaction is seen only in the A/B dimers and not in the C/C dimers. What was not immediately apparent from the NV structure was the additional flexibility possible between the P1 and P2 subdomains, which is quite evident in the present SMSV structure. The multiple points of flexibility could be an important factor in enhancing calicivirus diversity through structural variations within the context of a similar domain organization, somewhat akin to the interdomain flexibility seen in the antibody structures with a hinge and an elbow.

In the SMSV structure, in contrast to NV, the orientational changes between the S domain and the P1 subdomain excludes P1 to participate in the dimeric interactions. However, the additional flexibility between P1 and P2 brings the opposing P2 subdomains in the dimers to interact closely. Close interaction between the dimer-related P2 subdomains is consistently observed in all of the other caliciviruses thus far characterized by cryo-EM (26–28). It is quite plausible that the dimeric association of the P2 subdomain is a functional requirement, in that the initial receptor for calicivirus may be a dimer.

Comparison of the calicivirus sequences clearly indicates that the region that forms the P2 subdomain exhibits the most variability. Several earlier studies have implicated this region of the calicivirus sequence in antigenicity and possible receptor interactions (33–35, 41). Despite significant variation in the sequences, the basic polypeptide fold, with antiparallel β-strands, is conserved between SMSV and rNV. The main differences are in the loops that connect these strands. These loops can evidently tolerate significant sequence alterations without interfering with the basic polypeptide fold of this subdomain. Mapping of the neutralization epitopes to these loops in the distal P2 subdomain that can incorporate significant sequence and structural variations provides a mechanism by which antigenic diversity is achieved in caliciviruses. Although further studies are needed in regard to receptor identification for caliciviruses, the conserved region surrounded by these loops is a possible site for host-specific interactions, and its ability to tolerate sequence variations could be responsible for host diversity and suggested zoonotic potential.

In conclusion, we present here the x-ray structure of a native calicivirus from *Vesivirus* genus in the *Caliciviridae* family that exhibits a broad host range possibly including humans. Despite similar architectural design that is likely to be duplicated in all caliciviruses, our structural studies demonstrate how the modular organization of the capsid protein could be conducive to a wide diversity and host specificity associated with this family of viruses. The availability of the immunological data for some of the vesiviruses, which are not presently available for human caliciviruses, has allowed us to map epitopes onto a calicivirus structure. Structural mapping of the neutralization epitopes is likely applicable to human caliciviruses and may be useful for vaccine development and further mutational studies to gain insight into antigenicity and receptor interactions.

Materials and Methods

The crystal structure of SMSV was determined to 3.2-Å resolution by molecular replacement using a 19-Å cryo-EM map of SMSV (42) as an initial phasing model. Virus purification, crystallization, data collection, and the initial data processing, self-rotation function analysis were as described previously (42). A brief summary of crystal data and diffraction statistics is

provided in Table 1, which is published as supporting information on the PNAS web site. The phase refinement and extension were carried out by using real space averaging taking advantage of the fivefold noncrystallographic symmetry (43). The phase extension from 19 Å was carried out gradually in steps of one reciprocal lattice point by iterative cycles of molecular averaging with noncrystallographic fivefold symmetry, solvent flattening, and back transformation by using RAVE (44) and CCP4 (45). The model building and refinement was carried out iteratively by using the O (46) and CNS (47) suites of programs, respectively. The final R factor was 0.24, with an R_{free} of 0.26, for all of the observed reflections to 3.2-Å resolution. The stereochemistry of the final model was assessed by using PROCHECK (48), which indicated that 80% of the nonglycine residues were in the most favored region and none of the residues were in a disallowed region of the Ramachandran map. Other stereochemical characteristics of the three subunits were comparable with those of other structures determined to 3.0-Å resolution. The figures were made by using PYMOL (http://pymol.sourceforge.net) or RIBBONS (49).

We thank Dr. A. Radford for discussion and comments on the manuscript and the staff at Cornell High Energy Synchrotron Source, where the crystallographic data were collected on F1 beamline. This work was supported by National Institutes of Health Grant P01AI-57788 (to M.K.E. and B.V.V.P.) and a grant from the Welch Foundation (to B.V.V.P.).

1. Green, K. Y., Ando, T., Balayan, M. S., Berke, T., Clarke, I. N., Estes, M. K., Matson, D. O., Nakata, S., Neill, J. D., Studdert, M. J. & Thiel, H. J. (2000) *J. Infect. Dis.* **181,** Suppl. 2, S322–S330.
2. Hutson, A. M., Atmar, R. L. & Estes, M. K. (2004) *Trends Microbiol.* **12,** 279–287.
3. Fankhauser, R. L., Noel, J. S., Monroe, S. S., Ando, T. & Glass, R. I. (1998) *J. Infect. Dis.* **178,** 1571–1578.
4. Sugieda, M. & Nakajima, S. (2002) *Virus Res.* **87,** 165–172.
5. Smiley, J. R., Chang, K. O., Hayes, J., Vinje, J. & Saif, L. J. (2002) *J. Virol.* **76,** 10089–10098.
6. Guo, M., Chang, K. O., Hardy, M. E., Zhang, Q., Parwani, A. V. & Saif, L. J. (1999) *J. Virol.* **73,** 9625–9631.
7. Liu, B. L., Lambden, P. R., Gunther, H., Otto, P., Elschner, M. & Clarke, I. N. (1999) *J. Virol.* **73,** 819–825.
8. Widdowson, M. A., Rockx, B., Schepp, R., van der Poel, W. H., Vinje, J., van Duynhoven, Y. T. & Koopmans, M. P. (2005) *J. Med. Virol.* **76,** 119–128.
9. Radford, A. D., Gaskell, R. M. & Hart, C. A. (2004) *Curr. Opin. Infect. Dis.* **17,** 471–478.
10. Smith, A. W., Skilling, D. E., Cherry, N., Mead, J. H. & Matson, D. O. (1998) *Emerg. Infect. Dis.* **4,** 13–20.
11. Smith, A. W., Berry, E. S., Skilling, D. E., Barlough, J. E., Poet, S. E., Berke, T., Mead, J. & Matson, D. O. (1998) *Clin. Infect. Dis.* **26,** 434–439.
12. Hurley, K. F. & Sykes, J. E. (2003) *Vet. Clin. North Am. Small Anim. Pract.* **33,** 759–772.
13. Smith, A. W., Iversen, P. L., Skilling, D. E., Stein, D. A., Bok, K. & Matson, D. O. (2006) *J. Med. Virol.* **78,** 693–701.
14. Jiang, X., Wang, M., Graham, D. Y. & Estes, M. K. (1992) *J. Virol.* **66,** 6527–6532.
15. Lambden, P. R., Caul, E. O., Ashley, C. R. & Clarke, I. N. (1993) *Science* **259,** 516–519.
16. Prasad, B. V., Hardy, M. E., Dokland, T., Bella, J., Rossmann, M. G. & Estes, M. K. (1999) *Science* **286,** 287–290.
17. Guiver, M., Littler, E., Caul, E. O. & Fox, A. J. (1992) *J. Gen. Virol.* **73,** 2429–2433.
18. Matsuura, Y., Tohya, Y., Mochizuki, M., Takase, K. & Sugimura, T. (2001) *J. Gen. Virol.* **82,** 1695–1702.
19. Neill, J. D., Sosnovtsev, S. V. & Green, K. Y. (2000) *J. Virol.* **74,** 1079–1084.
20. Radford, A. D., Willoughby, K., Dawson, S., McCracken, C. & Gaskell, R. M. (1999) *J. Virol.* **73,** 8496–8502.
21. Tohya, Y., Yokoyama, N., Maeda, K., Kawaguchi, Y. & Mikami, T. (1997) *J. Gen. Virol.* **78,** 303–305.
22. Sosnovtsev, S. V., Belliot, G., Chang, K. O., Onwudiwe, O. & Green, K. Y. (2005) *J. Virol.* **79,** 4012–4024.
23. Glass, P. J., White, L. J., Ball, J. M., Leparc-Goffart, I., Hardy, M. E. & Estes, M. K. (2000) *J. Virol.* **74,** 6581–6591.
24. Clarke, I. N. & Lambden, P. R. (2000) *J. Infect. Dis.* **181,** Suppl. 2, S309–S316.
25. Sosnovtsev, S. V., Sosnovtseva, S. A. & Green, K. Y. (1998) *J. Virol.* **72,** 3051–3059.
26. Thouvenin, E., Laurent, S., Madelaine, M. F., Rasschaert, D., Vautherot, J. F. & Hewat, E. A. (1997) *J. Mol. Biol.* **270,** 238–246.
27. Prasad, B. V., Matson, D. O. & Smith, A. W. (1994) *J. Mol. Biol.* **240,** 256–264.
28. Chen, R., Neill, J. D., Noel, J. S., Hutson, A. M., Glass, R. I., Estes, M. K. & Prasad, B. V. (2004) *J. Virol.* **78,** 6469–6479.
29. Rossmann, M. G. & Johnson, J. E. (1989) *Annu. Rev. Biochem.* **58,** 533–573.
30. Carter, M. J., Milton, I. D., Turner, P. C., Meanger, J., Bennett, M. & Gaskell, R. M. (1992) *Arch. Virol.* **122,** 223–235.
31. Matsuura, Y., Tohya, Y., Onuma, M., Roerink, F., Mochizuki, M. & Sugimura, T. (2000) *J. Gen. Virol.* **81,** 195–199.
32. Harrison, S. C. (2001) *Curr. Opin. Struct. Biol.* **11,** 195–199.
33. Hutson, A. M., Chakravarty, S., Atmar, R. L., Prasad, B. V. V. & Estes, M. K. (2005) *Gastroenterology* **128,** A56–A56.
34. Tan, M., Hegde, R. S. & Jiang, X. (2004) *J. Virol.* **78,** 6233–6242.
35. Chakravarty, S., Hutson, A. M., Estes, M. K. & Prasad, B. V. (2005) *J. Virol.* **79,** 554–568.
36. Tohya, Y., Masuoka, K., Takahashi, E. & Mikami, T. (1991) *Arch. Virol.* **117,** 173–181.
37. Abad-Zapatero, C., Abdel-Meguid, S. S., Johnson, J. E., Leslie, A. G. W., Rayment, I., Rossmann, M. G., Suck, D. & Tsukihara, T. (1980) *Nature* **286,** 33–39.
38. Harrison, S. C., Olson, A. J., Schutt, C. E., Winkler, F. K. & Bricogne, G. (1978) *Nature* **276,** 368–373.
39. Hogle, J. M., Maeda, A. & Harrison, S. C. (1986) *J. Mol. Biol.* **191,** 625–638.
40. Fisher, A. J. & Johnson, J. E. (1993) *Nature* **361,** 176–179.
41. Lochridge, V. P., Jutila, K. L., Graff, J. W. & Hardy, M. E. (2005) *J. Gen. Virol.* **86,** 2799–2806.
42. Chen, R., Neill, J. D. & Prasad, B. V. (2003) *J. Struct. Biol.* **141,** 143–148.
43. Rossmann, M. G. (1972) *The Molecular Replacement Method* (Gordon & Breach, New York).
44. Read, R. J. & Kleywegt, G. J. (2001) in *Methods in Macromolecular Crystallography*, eds. Turk, D. & Johnson, L. (IOS, Amsterdam), pp. 123–135.
45. Collaborative Computational Project, Number 4 (1994) *Acta Crystallogr. D* **50,** 760–763.
46. Jones, T. A., Zou, J. Y., Xowan, S. W. & Kjeldgaard, M. (1991) *Acta Crystallogr. A* **47,** 392–400.
47. Brunger, A. T., Adams, P. D., Clore, G. M., DeLano, W. L., Gros, P., Grosse-Kunstleve, R. W., Jiang, J. S., Kuszewski, J., Nilges, M., Pannu, N. S., *et al*. (1998) *Acta Crystallogr. D* **54,** 905–921.
48. Lakowski, R. A., MacArthur, M. W., Moss, D. S. & Thornton, J. M. (1993) *J. Appl. Crystallogr.* **26,** 283–291.
49. Carson, M. (1997) in *Methods in Enzymology*, eds. Sweet, R. M. & Carter, C. W. (Academic, New York), Vol. 277, pp. 493–505.